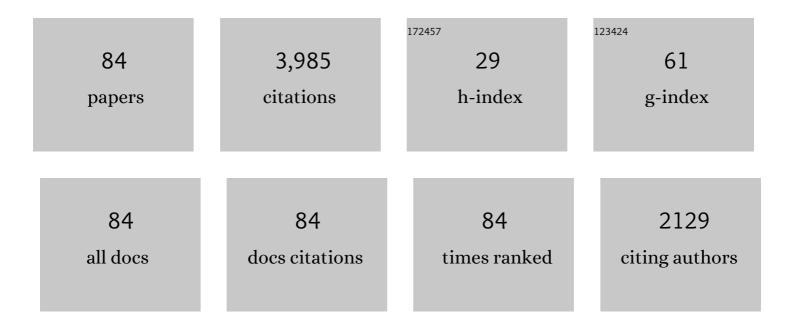
## Peter Stangeby

List of Publications by Year in descending order

Source: https://exaly.com/author-pdf/4076691/publications.pdf Version: 2024-02-01



#	Article	IF	CITATIONS
1	Separatrix-to-Wall Simulations of Impurity Transport with a Fully Three-Dimensional Wall in DIII-D. Fusion Science and Technology, 2023, 79, 36-45.	1.1	1
2	The role of B <sub>T</sub> -dependent flows on W accumulation at the edge of the confined plasma. Nuclear Fusion, 2022, 62, 026037.	3.5	6
3	Developing solid-surface plasma facing components for pilot plants and reactors with replenishable wall claddings and continuous surface conditioning. Part A: concepts and questions. Plasma Physics and Controlled Fusion, 2022, 64, 055018.	2.1	6
4	Developing solid-surface plasma facing components for pilot plants and reactors with replenishable wall claddings and continuous surface conditioning. Part B: required research in present tokamaks. Plasma Physics and Controlled Fusion, 2022, 64, 055003.	2.1	0
5	Comparison between SOLPS-4.3 and the Lengyel Model for ITER baseline neon-seeded plasmas. Nuclear Fusion, 2021, 61, 046029.	3.5	8
6	First evidence of dominant influence of E × B drifts on plasma cooling in an advanced slot divertor for tokamak power exhaust. Nuclear Fusion, 2021, 61, 054002.	3.5	15
7	Modeling of ExB effects on tungsten re-deposition and transport in the DIII-D divertor. Nuclear Fusion, 2021, 61, 096018.	3.5	13
8	Numerical assessment of the new V-shape small-angle slot divertor on DIII-D. Nuclear Fusion, 2021, 61, 116042.	3.5	17
9	The role of divertor pumping in plasma detachment and particle exhaust in a closed divertor. Nuclear Fusion, 2021, 61, 016022.	3.5	13
10	The roles of power loss and momentum-pressure loss in causing particle-detachment in tokamak divertors: II. 2 Point Model analysis that includes recycle power-loss explicitly. Plasma Physics and Controlled Fusion, 2020, 62, 025013.	2.1	13
11	Reproduction of collector probe deposition profiles using the far-SOL impurity transport code 3DLIM. Nuclear Materials and Energy, 2020, 25, 100811.	1.3	6
12	A simple analytic model of impurity leakage from the divertor and accumulation in the main scrape-off layer. Nuclear Fusion, 2020, 60, 106005.	3.5	25
13	Evaluation of the impact of divertor closure on high-Z material transport and leakage in small angle slot divertor with toroidal tungsten rings in DIII-D. Physica Scripta, 2020, T171, 014072.	2.5	10
14	Localized divertor leakage measurements using isotopic tungsten sources during edge-localized mode-y H-mode discharges on DIII-D. Nuclear Fusion, 2020, 60, 016028.	3.5	13
15	The roles of power loss and momentum-pressure loss in causing particle-detachment in tokamak divertors: I. A heuristic model analysis. Plasma Physics and Controlled Fusion, 2020, 62, 025012.	2.1	15
16	Net versus gross erosion of silicon carbide in DIII-D divertor. Physica Scripta, 2020, T171, 014064.	2.5	5
17	SOLPS analysis of changes in the main SOL of DIII-D associated with divertor detachment vs attachment and closure vs openness. Nuclear Fusion, 2020, 60, 056011.	3.5	17
18	Manipulation of E×B drifts in a slot divertor with advanced shaping to optimize detachment. Nuclear Fusion, 2020, 60, 126030	3.5	13

#	Article	IF	CITATIONS
19	Impact of ELM control techniques on tungsten sputtering in the DIII-D divertor and extrapolations to ITER. Physics of Plasmas, 2019, 26, .	1.9	19
20	Physics basis for the first ITER tungsten divertor. Nuclear Materials and Energy, 2019, 20, 100696.	1.3	307
21	Modeling of inter- and intra-edge-localized mode tungsten erosion during DIII-D H-mode discharges. Nuclear Fusion, 2019, 59, 126018.	3.5	10
22	Use of isotopic tungsten tracers and a stable-isotope-mixing model to characterize divertor source location in the DIII-D metal rings campaign. Nuclear Materials and Energy, 2019, 19, 358-363.	1.3	13
23	First experimental tests of a new small angle slot divertor on DIII-D. Nuclear Fusion, 2019, 59, 086054.	3.5	49
24	Dependence of neutral pressure on detachment in the small angle slot divertor at DIII-D. Nuclear Materials and Energy, 2019, 19, 487-492.	1.3	24
25	Evidence of near-SOL tungsten accumulation using a far-SOL collector probe array and OEDCE modelling in the DIII-D metal rings L-mode discharges. Nuclear Materials and Energy, 2019, 19, 287-294.	1.3	19
26	Basic physical processes and reduced models for plasma detachment. Plasma Physics and Controlled Fusion, 2018, 60, 044022.	2.1	124
27	Experimental validation of a model for particle recycling and tungsten erosion during ELMs in the DIII-D divertor. Nuclear Materials and Energy, 2018, 17, 164-173.	1.3	22
28	Utilization of outer-midplane collector probes with isotopically enriched tungsten tracer particles for impurity transport studies in the scrape-off layer of DIII-D (invited). Review of Scientific Instruments, 2018, 89, 10I115.	1.3	18
29	Measurement and modeling of aluminum sputtering and ionization in the DIII-D divertor including magnetic pre-sheath effects. Nuclear Fusion, 2018, 58, 106019.	3.5	8
30	Experimentally-based ExB drifts in the DIII-D divertor and SOL calculated from integration of Ohm's law using Thomson scattering measurements of Te and ne. Nuclear Materials and Energy, 2017, 12, 876-881.	1.3	8
31	SOLPS analysis of neutral baffling for the design of a new diverter in DIII-D. Nuclear Fusion, 2017, 57, 056043.	3.5	41
32	Characterizing Low-Z erosion and deposition in the DIII-D divertor using aluminum. Nuclear Materials and Energy, 2017, 12, 441-446.	1.3	5
33	DiMES PMI research at DIII-D in support of ITER and beyond. Fusion Engineering and Design, 2017, 124, 196-201.	1.9	18
34	OEDGE modeling for the planned tungsten ring experiment on DIII-D. Nuclear Materials and Energy, 2017, 12, 755-761.	1.3	10
35	The inter-ELM tungsten erosion profile in DIII-D H-mode discharges and benchmarking with ERO+OEDGE modeling. Nuclear Fusion, 2017, 57, 056034.	3.5	47
36	Measurements of tungsten migration in the DIII-D divertor. Physica Scripta, 2017, T170, 014041.	2.5	10

#	Article	IF	CITATIONS
37	Strong correlation between <i>D</i> <sub>2</sub> density and electron temperature at the target of divertors found in SOLPS analysis. Nuclear Fusion, 2017, 57, 056007.	3.5	44
38	Simulation of gross and net erosion of high-Z materials in the DIII-D divertor. Nuclear Fusion, 2016, 56, 016021.	3.5	41
39	Measurements of gross erosion of Al in the DIII-D divertor. Journal of Nuclear Materials, 2015, 463, 810-813.	2.7	7
40	Electron pressure balance in the SOL through the transition to detachment. Journal of Nuclear Materials, 2015, 463, 533-536.	2.7	56
41	Identifying the location of the OMP separatrix in DIII-D using power accounting. Nuclear Fusion, 2015, 55, 093014.	3.5	35
42	Control of high-Z PFC erosion by local gas injection in DIII-D. Journal of Nuclear Materials, 2015, 463, 605-610.	2.7	9
43	Material migration studies with an ITER first wall panel proxy on EAST. Nuclear Fusion, 2015, 55, 023013.	3.5	35
44	Impact of a narrow limiter SOL heat flux channel on the ITER first wall panel shaping. Nuclear Fusion, 2015, 55, 033019.	3.5	54
45	Analysis of a tungsten sputtering experiment in DIII-D and code/data validation of high redeposition/reduced erosion. Fusion Engineering and Design, 2015, 94, 67-71.	1.9	25
46	Influence of theE  ×  Bdrift in high recycling divertors on target asymmetries. Plasma Physics a Controlled Fusion, 2015, 57, 095002.	and 2.1	56
47	Net versus gross erosion of high- <i>Z</i> materials in the divertor of DIII-D. Physica Scripta, 2014, T159, 014030.	2.5	23
48	Progress in the physics basis of a Fusion Nuclear Science Facility based on the Advanced Tokamak concept. Nuclear Fusion, 2014, 54, 073015.	3.5	33
49	Experimental Advanced Superconducting Tokamak/material and plasma evaluation system material migration experiment. Physica Scripta, 2014, T159, 014069.	2.5	8
50	A full tungsten divertor for ITER: Physics issues and design status. Journal of Nuclear Materials, 2013, 438, S48-S56.	2.7	618
51	An experimental comparison of gross and net erosion of Mo in the DIII-D divertor. Journal of Nuclear Materials, 2013, 438, S309-S312.	2.7	22
52	Measurements of net erosion and redeposition of molybdenum in DIII-D. Journal of Nuclear Materials, 2013, 438, S822-S826.	2.7	20
53	The effect of thermo-oxidation on plasma performance and in-vessel components in DIII-D. Nuclear Fusion, 2013, 53, 073008.	3.5	11
54	The Chodura sheath for angles of a few degrees between the magnetic field and the surface of divertor targets and limiters. Nuclear Fusion, 2012, 52, 083012.	3.5	77

#	Article	IF	CITATIONS
55	ERO code benchmarking of ITER first wall beryllium erosion/re-deposition against LIM predictions. Physica Scripta, 2011, T145, 014008.	2.5	38
56	Modelling of beryllium erosion–redeposition on ITER first wall panels. Journal of Nuclear Materials, 2011, 415, S165-S169.	2.7	57
57	Assessing material migration through 13C injection experiments. Journal of Nuclear Materials, 2011, 415, S278-S283.	2.7	30
58	Physics basis and design of the ITER plasma-facing components. Journal of Nuclear Materials, 2011, 415, S957-S964.	2.7	361
59	Obtaining reactor-relevant divertor conditions in tokamaks. Nuclear Fusion, 2011, 51, 063001.	3.5	47
60	A three-dimensional analytic model for discrete limiters in ITER. Nuclear Fusion, 2010, 50, 035013.	3.5	10
61	Overview of the recent DiMES and MiMES experiments in DIII-D. Physica Scripta, 2009, T138, 014007.	2.5	20
62	Indications of an inward pinch in the inner SOL of DIII-D from 13C deposition experiments. Journal of Nuclear Materials, 2009, 390-391, 376-379.	2.7	9
63	Plasma interactions with the outboard chamber wall in DIII-D. Journal of Nuclear Materials, 2009, 390-391, 785-788.	2.7	8
64	Analysis for shaping the ITER first wall. Journal of Nuclear Materials, 2009, 390-391, 963-966.	2.7	26
65	A possible role of radial electric field in driving parallel ion flow in scrape-off layer of divertor tokamaks. Nuclear Fusion, 2007, 47, 762-772.	3.5	39
66	Transport and deposition of 13C from methane injection into partially detached H-mode plasmas in DIII-D. Journal of Nuclear Materials, 2007, 363-365, 72-77.	2.7	24
67	OEDGE modeling of the DIII-D H-mode 13CH4 puffing experiment. Journal of Nuclear Materials, 2007, 363-365, 140-145.	2.7	17
68	Particle and parallel momentum balance equations with inclusion of drifts, for modelling strong- to weakly-collisional edge plasmas. Nuclear Fusion, 2006, 46, 975-993.	3.5	5
69	Re-construction of detached divertor plasma conditions in DIII-D using spectroscopic and probe data. Journal of Nuclear Materials, 2005, 337-339, 256-260.	2.7	23
70	13C transport studies in L-mode divertor plasmas on DIII-D. Journal of Nuclear Materials, 2005, 337-339, 30-34.	2.7	38
71	Far scrape-off layer and near wall plasma studies in DIII-D. Journal of Nuclear Materials, 2005, 337-339, 717-721.	2.7	15
72	DIVIMP modeling of the toroidally symmetrical injection of 13CH4 into the upper SOL of DIII-D. Journal of Nuclear Materials, 2005, 337-339, 124-128.	2.7	27

#	Article	IF	CITATIONS
73	The magnitude of plasma flux to the main-wall in the DIII-D tokamak. Plasma Physics and Controlled Fusion, 2005, 47, 1579-1607.	2.1	40
74	Far SOL transport and main wall plasma interaction in DIII-D. Nuclear Fusion, 2005, 45, 1589-1599.	3.5	123
75	Interpretive modeling of simple-as-possible-plasma discharges on DIII-D using the OEDGE code. Journal of Nuclear Materials, 2003, 313-316, 883-887.	2.7	65
76	Effects of divertor geometry and chemical sputtering on impurity behaviour and plasma performance in JET. Nuclear Fusion, 2000, 40, 379-396.	3.5	28
77	Experimental divertor physics. Plasma Physics and Controlled Fusion, 1997, 39, 779-930.	2.1	349
78	Impurity retention by divertors. I. One dimensional models. Nuclear Fusion, 1995, 35, 1391-1412.	3.5	70
79	Can detached divertor plasmas be explained as self-sustained gas targets?. Nuclear Fusion, 1993, 33, 1695-1705.	3.5	124
80	Calculation of observable quantities using a divertor impurity interpretive code, DIVIMP. Journal of Nuclear Materials, 1992, 196-198, 258-263.	2.7	123
81	Impurity transport at the plasma edge. Journal of Nuclear Materials, 1990, 176-177, 51-64.	2.7	17
82	Monte Carlo modelling of impurity ion transport for a limiter source/sink. Nuclear Fusion, 1988, 28, 1945-1962.	3.5	83
83	Interpretation of Langmuir, heat-flux, deposition, trapping and gridded energy analyser probe data for impure plasmas. Journal Physics D: Applied Physics, 1987, 20, 1472-1478.	2.8	23
84	Interpretation of plasma impurity deposition probes. Analytic approximation. Physics of Fluids, 1987, 30, 3262.	1.4	24